Asynchronous Motor Imagery BCI and LiDAR-Based Shared Control System for Intuitive Wheelchair Navigation

Jin Woo Choi, Junyong Park, Sejoon Huh, and Sungho Jo

Abstract—**Mapping drivers' thoughts directly to mobility system control would make driving more intuitive as if the mobility system is an extension of their own body. Such a system would allow patients with motor disabilities to drive, as it would not require any physical movement. In this article, we therefore propose a brain-controlled mobility system that analyzes real-time neural signals elicited from motor imagery, an imagination of different body movements. As such asynchronous brain–computer interfaces (BCIs) are prone to error, our system contains shared control capabilities that take into consideration continuously updated information of the surrounding environment along with electroencephalogram (EEG) signals to improve navigating performance without precise and accurate control from the driver. With our shared control method that uses a wheelchair with light detection and ranging (LiDAR) and inertial measurement unit (IMU) sensors, we held a comparative study in which participants drove our wheelchair with and without our shared control approach using either our brain-controlled system or a keyboard in a physical environment. The experimental results show that among the five participants, the three participants that failed the driving task with the asynchronous BCI-based system could also successfully complete it using our shared control approach. Furthermore, our approach narrows the gap between driving with neural signals and driving with a widely used interface in terms of both elapsed time and safety. These results show not only the potential of brain signals for driving but also the applicability of BCIs to real-life situations.**

Index Terms—**Brain–computer interface (BCI), electroencephalogram (EEG), light detection and ranging (LiDAR), motor imagery, shared control.**
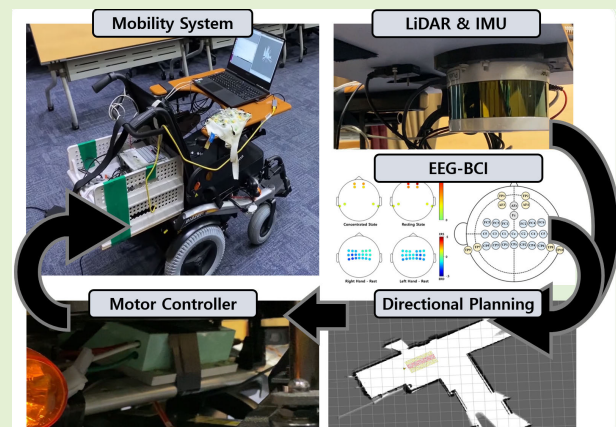
I. INTRODUCTION

ASSISTIVE devices for users with motor disabilities support daily activities by executing or supporting intended actions. Such devices aim to replace the disabled body part, imitating its functionality, and allowing users to feel them as a natural extension of their own. One of the rising research areas in this field is brain–computer interfaces (BCIs). BCIs analyze neural activities from the brain to discriminate user intentions and translate the corresponding brain signals into device commands. With their inherent independence from movement, BCIs are applicable to various applications for patients with motor disabilities [1], [2]. Of the many noninvasive methods to analyze neural activity in real-time, electroencephalogram (EEG) has been widely applied to control numerous types of devices such as humanoid robots, robotic arms, brain-controlled keyboards, and simulations conducted with virtual reality head-mounted displays [3], [4], [5], [6].

Moving from one location to another being an essential component of daily life activities, BCIs have also been applied to various systems to support users' mobility [7], [8]. As one of the widely used real-life devices that assist individualized mobility, wheelchairs with BCIs were used as prototypes for brain-actuated personal mobility systems in previous studies. Some of the work uses motor imagery
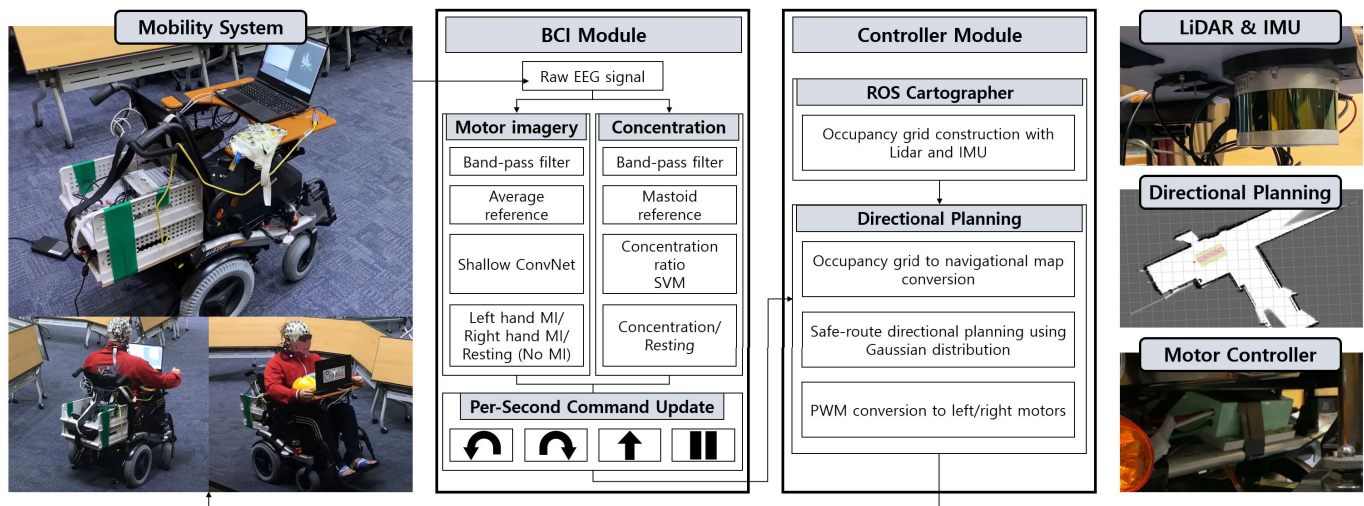
Fig. 1. Overview of our mobility system. The BCI module converts real-time brain signals into a command each second. The controller module executes the command along with the perceived environmental information. The drivers are seated in the mobility system as they control it.

to control a wheelchair. Such studies include work by Yu et al. [10] in which a wheelchair changed its movement by having users perform different combinations of left-hand and right-hand motor imagery, effectively allowing asynchronous control with six steering functions. Another instance from Zhang et al. [9] used a motor imagery-based BCI to select a predefined destination within a familiar environment and addressed its successful integration with automated wheelchair navigation, eliminating the need for additional commands. There have also been studies that use reactive brain signals to determine the driver's intention with greater discrimination performance than those using motor imagery. For instance, Sakkalis et al. [11] proposed a wheelchair system that utilized steady-state visually evoked potentials (SSVEPs) presented through augmented reality glasses for wheelchair control, receiving positive user feedback regarding its usability. Another work by Kim et al. [12] utilized vibrotactile stimuli placed on the hands and feet to control a wheelchair with evoked brain signals, resulting in improved navigation with enhanced BCI performance compared with motor imagery alone. Reactive brain responses from different types of stimuli have frequently been used in other studies to facilitate reliable wheelchair navigation [13], [14], [15].

Despite ongoing research, existing BCI-based mobility systems have limitations that make them difficult to use in real settings. Previous methods that drive mobility in real-world environments utilize various types of stimuli, use sequences of multiple different brain signals per a single movement change, rely on synchronous control methods that only permit user commands in some predefined circumstances, or utilize automated driving with predefined map information. Although such methods may redeem the error-prone problem of previous BCI-based mobility systems, these methods are either less intuitive or may restrict the user's authority of control over the system [16], [17]. Ideally, a new driving system would be free from such limitations. The interface should intuitively map thoughts into actions as motor imagery-based systems while also exhibiting high control performance and ensuring

the driver's authority over the system. These implementations would make driving feel as if the system was a natural extension of the body, able to be controlled simply by the thought of moving. As assistive devices designed to support individual movements, mobility systems should maximize the driver's safety, use asynchronous control such that drivers are able to freely command the system throughout the entire operating period, and be applicable to various circumstances even without prior information of the surrounding environment.

Our study aims to take a step toward this ideal driving system by presenting an asynchronously driven shared control mobility that continuously and intuitively maps the driver's thoughts into the left rotation, right rotation, forward movement, and stopping the movement, as shown in Fig. 1. With a major component of our interface being a motor imagery-based BCI, our system directly maps the driver's thoughts to control without any form of stimulus. Unlike other studies where synchronous control, preexisting environmental information, or multiple different selections for a single movement was alternatively used to rectify the high error rate of motor imagery, we used information from light detection and ranging (LiDAR) and inertial measurement unit (IMU) sensors to keep the driver on the desired path despite minor motor imagery discrimination errors. Our proposed shared control policy therefore preserves the driver's freedom of control and does not require precise directional adjustments from the user. To provide evidence that our method has potential for real applications, our mobility system was also constructed as a form of a motorized wheelchair, and the experiments with different control conditions were conducted with the driver in the wheelchair as they controlled it. In light of this, the following summary highlights the contributions of this work.

1) We proposed a shared control approach that utilizes asynchronous BCI to continuously map users' thoughts into device commands while using the perceived environmental information from LiDAR and IMU sensors to rectify the error-prone problem of BCI.
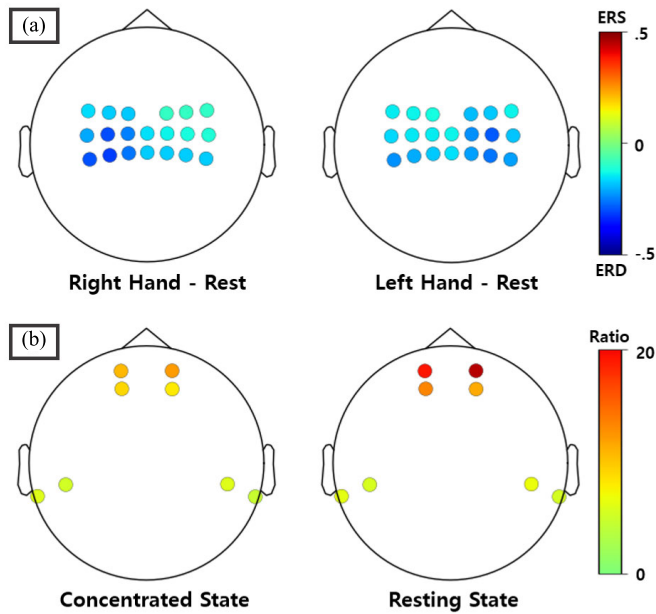
Fig. 2. Average brain activity patterns of our participants for the motor imagery and concentration tasks. (a) Change in oscillatory brain signals, between motor imagery and resting states. (b) Difference in concentration ratio between concentration and resting states.

2) A mobility system driven by our shared control capabilities was constructed, and experiments with different control conditions were conducted in a real-world setting to analyze and compare their navigation performance.

The rest of this article is organized as follows. Section II introduces an implementation of our brain-controller interface which discriminates motor imagery and concentration states of users. Section III proposes our shared control design in detail. Section IV describes our experiment containing user training and the driving tasks. Section V presents the results of our experiment. Finally, Sections VI and VII convey the discussion and conclusion of this study.

II. BRAIN-CONTROLLER INTERFACE

As our mobility system utilizes signals from brain activities during motor imagery and concentration, it is necessary to train our system to analyze different brain activities of drivers performing different tasks. When motor imagery is performed, a degradation of brain activity oscillation known as event-related desynchronization (ERD) occurs in the sensorimotor areas, mainly from the region corresponding to the imagined movement [18], [19]. As shown in Fig. 2(a), performing motor imagery of hand movement is known to elicit ERD patterns in the contralateral sensorimotor area. On the other hand, as shown in Fig. 2(b), the concentration state of the drivers can be measured from the frontal cortex, where different frequency ranges of brain activity related to different mental states. For concentration, the alpha, beta, and theta bands are known to be closely related as alpha and theta correspond to relaxation, and beta to arousal and alertness [20]. Our system therefore constructs classification models to learn and discriminate driver intentions using their brain patterns.
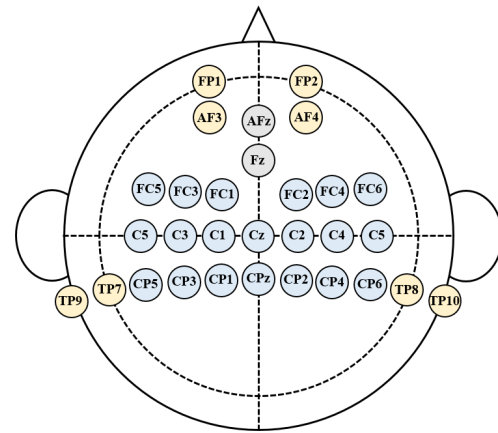
Fig. 3. Electrode positions used in our study. Electrodes in blue were used to discriminate motor imagery states. Electrodes in yellow were used to discriminate the concentrated state of users. Electrodes in gray are the ground and reference positions.

A. Signal Acquisition and Processing

BrainProducts' actiChamp and actiCAP (BrainProducts, Munich, Germany) were used to record EEG data, which was subsequently used to make classification models that analyzed brain patterns and converted them into commands for the controller module. As shown in Fig. 3, a total of 30 active electrodes from the frontal cortex, sensorimotor cortex, and mastoid positions were used according to the international 10–20 system. The ground and reference electrodes were located at positions AFz and Fz, respectively. The data were sampled at a rate of 500 Hz and the impedance of each electrode was kept under 10 kΩ to gather high-quality signals.

B. EEG Classification

For the classification method used to convert real-time EEG signals into the driving command once per every second, we used two different classification models simultaneously: one to classify motor imagery and the other to classify the concentration state. For the motor imagery classification model, we used a ShallowConvNet model [21], a widely used state-of-the-art deep learning architecture that extracts oscillatory features and spatial patterns for EEG analysis. For the concentration model, we applied a support vector machine (SVM) [22] on the concentration ratio computed with the EEG data of the frontal cortex.

1) Motor Imagery Classification: The EEG data from the sensorimotor cortex (FC5, C5, CP5, FC3, C3, CP3, FC1, C1, CP1, Cz, CPz, FC2, C2, CP2, FC4, C4, CP4, FC6, C6, and CP6) were used to classify motor imagery tasks. For signal preprocessing, an 8–36-Hz bandpass filter was applied to the data. As most of the EEG data for training the model was gathered on a different day to prevent participants from being fatigued, average referencing was further applied to the data.

The ShallowConvNet used for our experiment takes the most recent 2-s window of EEG data and classifies it into one of three motor imagery states: left hand, right hand, and resting state. As described in Fig. 4, the ShallowConvNet architecture contains two convolutional layers for temporal and spatial filtering, followed by a squaring nonlinearity, average pooling,
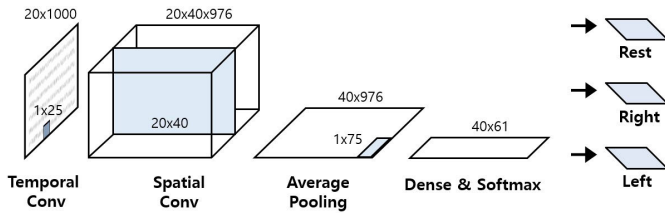
Fig. 4. ShallowConvNet architecture used in this study to classify 2-s-long EEG signals into a resting state, left-hand, or right-hand motor imagery.

logarithmic activation, and a dense layer with softmax to consider diverse band power ranges within multiple electrodes used for discriminating motor imagery states.

2) Concentration State Classification: The EEG data from the frontal cortex (FP1, FP2, AF3, and AF4) and mastoid region (TP7, TP8, TP9, and TP10) were used to classify the concentration state. To calculate the concentration ratio from each electrode, a 1–40-Hz bandpass filter was applied to the data. A rereferencing of the EEG data from the frontal cortex was applied using the mastoid electrodes.

The classification model for concentration state also used the most recent 2-s window of EEG data. As previous studies reported that changes in theta, alpha, and beta waves are associated with the concentration and resting state of users [20], [23], the power spectral densities (PSDs) of these three different frequency bands were used to calculate the concentration ratio from each electrode

$$\text{concentration} = (\theta + \alpha)/\beta \qquad (1)$$

where θ, α, and β represent PSD values calculated from the frequency ranges of 4–8, 8–12, and 12–30 Hz, respectively. The four different concentration ratios calculated from the four frontal electrodes were then used to construct the SVM concentration model.

3) Generation of Commands for Mobility System: The last 2-s window of EEG data was used to classify both motor imagery and concentration state in a parallel manner, producing a single command per second. Whenever motor imagery was classified as left-hand or right-hand movement, the mobility system turned toward the corresponding direction. Whenever motor imagery was classified as resting state, the mobility system either moved forward or stopped moving depending on whether the driver was classified to be concentrating or not, respectively. To account for misclassification, the system required at least two consecutive matching commands before executing a movement, otherwise it maintained its previous movement. The system also stopped moving for the user's safety when three consecutive commands were all different. This implementation took into account the possibility that such instances could be attributed to either the unreliability of the processed brain signals or the user's confusion in determining the next movement to perform.

III. INTELLIGENCE-ASSISTED CONTROL DESIGN

Along with the commands continuously generated through our brain-controller interface module, the surrounding map information from the LiDAR and IMU sensors was used to compensate for BCI's error-prone problem. Our approach to shared control consists of three primary components. First, the construction of the navigational map, which assigns values to each grid indicating the safety of the corresponding area based on the distance to the nearest obstacle. Second, directional planning, which adjusts the directional path the mobility system should take by considering the safety of the movement direction in addition to the user's initially controlled direction. Finally, the directional path follower aims to refine the system's movement from the continuously adjusted directional path. In this section, we introduce our shared control method of using the two aforementioned sensors and our brain-controller interface module in detail.

A. Simultaneous Localization and Mapping Using LiDAR and IMU

Robot operating system (ROS) kinetic was used to integrate our mobility system with a map of the surrounding environment that also contains previously navigated paths. Our interface used Velodyne LiDAR PUCK (VLP-16) and Microstrain's 3DM-GX5-25 IMU sensors attached to a 2-D Cartographer simultaneous localization and mapping (SLAM) system to track the position and orientation of the mobility system [24]. The perceived position and orientation information of the system from the Cartographer was used to design our shared control method. The map of the surrounding environment was also continuously merged with the previously collected information and updated in the controller module.

B. Navigational Map Construction

The controller module made several modifications from the continuously updated occupancy grid acquired through ROS, which contained integer values ranging from 0 to 100 indicating how confident the system was of occupied regions. Using the breadth-first search (BFS) algorithm, the occupancy grid was transformed into a distance map, with each location being assigned a label indicating the distance between it and the nearest occupied region. The regions labeled as occupied were those with a confidence level above a specified threshold on the occupancy grid.

This distance map was then finally converted into a navigational map. The navigational map was constructed by multiplying each region of the distance map by the difference between its confidence level on the occupancy grid and 100, the highest possible confidence level. Since the difference can be seen as the likeliness of vacancy, a higher value on this navigational map therefore represented a higher chance of the corresponding area being vacant and further away from nearby obstacles. This navigational map was then used for directional planning to search for a path that minimizes the chances of collision.

C. Gaussian Distribution-Based Directional Planning

To ensure safe navigation and rectify unstable paths due to inaccuracies from the asynchronous BCI, we devised a directional path planning method based on probability distributions using the continuously updated navigational map. The method

aims to avoid collision and estimate the driver's intended path despite imprecise control from the BCI module. This planning was activated whenever the forward command was accordingly sent to the controller module as either the first command of operation or the command following a rotation command. The initial path was set as a straight line from the mobility system's position toward the direction it faced at the time of the command. The desired path was updated as the mobility system's position changed within Cartographer to account for obstacles encountered near the initial path.

First, the closest point (i, j) on the initial directional path from the current position of the mobility system, or the projection of the position of the mobility system onto the path, was calculated using the following equation:

$$i = x_t \cos^2\theta + (y_t - y_0) \sin\theta\cos\theta + x_0\sin^2\theta$$
$$j = y_t \sin^2\theta + (x_t - x_0) \sin\theta\cos\theta + y_0\cos^2\theta \qquad (2)$$

where t represents time, (x_0, y_0) is the starting position of the desired path, θ is the angle counterclockwise from the x-axis of the map to the path, and (x_t, y_t) is the current position of the mobility system. This is done in order to disregard minor differences between the actual position of the mobility system and the initial path, as the actual position may not be on the path (as will be discussed in Section III-D regarding positional proportional–integral–differential (PID) control).

This projected position was then used to update the path the mobility system should follow by calculating the scores of the possible linear paths from the current point. Scores of the paths from $-90°$ to $90°$ away from the initial path with a step interval of $2°$ were calculated as follows given the values from the navigational map:

$$S(\phi) = \sum_{l=0}^{l_\phi} \sum_{w=-w_p}^{w_p} N(i + l\cos\phi - w\sin\phi, \, j + l\sin\phi + w\cos\phi)$$
$$\{\phi \in 2\mathbb{Z} | \theta - 90 \le \phi \le \theta + 90\} \qquad (3)$$

where l_ϕ represents the distance to the first obstacle when taking path ϕ, w_p is a predetermined half-width for every path to account for the system not staying directly on the path during PID control, and N is the latest version of the navigational map. Thus, each score for some ϕ is a summation of all values in the navigational map that belong to the rectangular area that has a starting edge with midpoint (i, j) and an ending edge at the first obstacle encountered when moving toward ϕ.

In order to prioritize the direction of the initial path, as that direction was where the driver intended to drive toward and to penalize directions that differ greatly from the initial direction [25], the range of angles was mapped to a Gaussian distribution

$$\mathcal{N}(\phi; \mu, \sigma) = \frac{1}{\sqrt{2\pi\sigma^2}} \exp\left[-(\phi - \mu)^2 / 2\sigma^2\right] \qquad (4)$$

where μ and σ represent the mean and standard deviation of the Gaussian distribution, respectively. The calculated Gaussian probability was then multiplied by the previously calculated scores for the possible paths, and the direction with the greatest score was chosen to be the new path as seen in the following equation:

$$\text{rot} = \arg\max_\phi S(\phi) \cdot \mathcal{N}(\phi; \theta, \pi/6). \qquad (5)$$

Thus, by applying the parameters θ and $\pi/6$ to the Gaussian distribution, the equation prioritizes setting the initial path direction as the highest priority, penalizes directions further from the initial path, and considers primarily the range from $-90°$ to $90°$ from the initial direction.

D. Positional PID-Based Directional Path Follower

While our directional planning may continuously update the direction the mobility system should move along with constantly changing information it perceived, immediately positioning the mobility system to such frequently changing direction may cause jerky movements that may adversely affect the status of drivers as well as the performance of BCI.

To smoothly direct our mobility system to a desired path that may continuously change, we additionally formulated a positional PID-based directional path follower inspired by the conventional PID motor control [26]. We first calculated the error of the current position with respect to some desired paths as follows:

$$\text{err}(t) = (x_t - x_0) \sin\theta - (y_t - y_0) \cos\theta \qquad (6)$$

where the variables mentioned in the equation have the same definitions as those from Section III-C. Thus, the error rate was defined by the perpendicular distance between the desired path and the current position of the mobility system. This error was updated at a frequency of 50 Hz, which was determined considering the specifications of the used sensors. Furthermore, the sign of the error rate provides information on whether the current position was to the left or right side of the desired path, which can then be used to decide which motor should be quickened to adjust the direction of the mobility system.

Then, the PID value was calculated using the following equation:

$$\text{pid}(t) = K_p |\text{err}(t)| + K_i \int_0^t |\text{err}(t)| dt + K_d \frac{d}{dt} |\text{err}(t)| \qquad (7)$$

where K_p, K_i, and K_d are PID coefficients indicating proportional, integral, and derivative parameters, respectively. These parameters were adjusted by trial and error with varying weights placed on the mobility system and remained unchanged for all participant experiments.

The pulsewidth modulation (PWM) for left-hand and right-hand motors were therefore determined as follows:

$$(v_l, v_r) = \begin{cases} (v_f + \min(v_{\max}, \text{pid}(t)), v_f), & \text{err}(t) < 0 \\ (v_f, v_f + \min(v_{\max}, \text{pid}(t))), & \text{err}(t) > 0 \\ (v_f, v_f), & \text{otherwise} \end{cases} \qquad (8)$$

where v_f represents a preselected initial velocity for forward movement, and $v_{\max}$ is a preselected maximum threshold for velocity. With this control approach, the mobility system
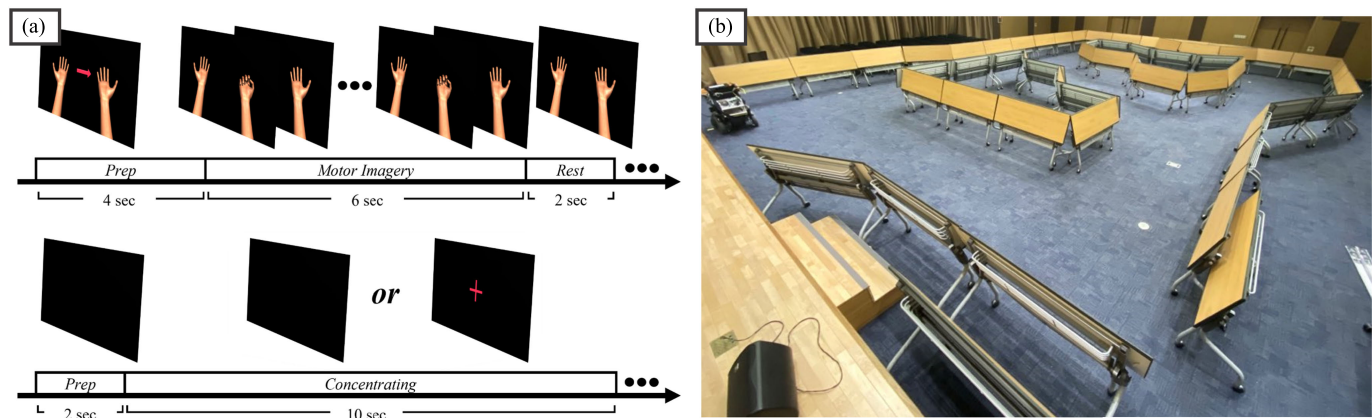
Fig. 5. (a) Flow of the training tasks during the motor imagery and concentration training sessions. (b) Figure-8 track we used for the driving experiments. Participants were to freely and continuously command the mobility system as they followed the informed 8-shaped path.

could follow the desired path computed by the directional planning method using the positional information updated by Cartographer as feedback.

E. Collision Avoidance

In order to avoid collisions, a distance threshold was selected. If the mobility system was within the threshold of an obstacle, the mobility system would automatically stop and only allow further commands that would increase the distance from the obstacle. For rotation commands in such cases, the mobility system only performed rotations in place. Similar policies were applied to forward commands. If an obstacle was detected within the threshold but another path was determined through directional planning to avoid a collision, the system turned in place to direct the system toward the newly found path. We applied such a metric in all our driving experiments to ensure the safety of participants.

IV. EXPERIMENT

To evaluate our mobility system and our shared control method, we recruited participants and asked them to drive our system through a given track. In our experiment, participants were to perform user training for our brain-controller interface module and were asked to control our mobility system using four different control conditions.

A. Participants

Five healthy male participants aged between 23 and 26 drove our mobility system. Prior to the experiment, all participants were informed about the experimental procedures and gave their written consent.

B. User Training for EEG Classification Model Construction

As brain signals vary between individuals, training the model with the EEG data collected from each participant is an essential procedure for BCI applications. Prior to our experiment, participants went through user training in which their EEG data for motor imagery and concentration tasks were collected and used for constructing the model.

The user training was split into two sittings, with each sitting corresponding to one of the two models and the motor imagery training preceding the concentration training, as shown in Fig. 5(a). The user training was held in a soundproof room to collect high-quality brain signals from participants in an environment with minimal distractions. Participants were seated in a comfortable chair in front of a desk with a monitor screen and were instructed to gaze and follow the instructions shown on the monitor screen.

1) Motor Imagery Training: The motor imagery training consisted of multiple sessions, with each session consisting of ten consecutive motor imagery trials. A single motor imagery trial consisted of three different tasks in a randomized order: left-hand grasping motor imagery, right-hand grasping motor imagery, and resting.

Each task was a sequence of a 4-s preparation period, a 6-s motor imagery period, and a 2-s resting period. In the preparation period, either a cross cue indicating the resting task or an arrow cue indicating the left or right task was shown on the monitor screen. In the motor imagery period, participants were instructed to perform the motor imagery task, and virtual hands executing the motor imagery task were also shown on the monitor screen to support imagery. Finally, in the resting period, participants were expected to rest with minimal movements such as eye blinks permitted. In the preparation and motor imagery periods, participants were asked to avoid movements including eye blinking and muscle movements as much as possible.

Participants performed at least six training sessions and were encouraged up to two additional sessions if they were not fatigued.

2) Concentration Training: The concentration training consisted of three sessions, with each session consisting of ten consecutive concentration trials. A single trial consisted of two different tasks in a randomized order: concentration and resting.

Each task was a sequence of a 2-s preparation period and a 10-s concentrating period. During the preparation period, participants were allowed to make minimal movements such as eye blinking to prevent eye fatigue. In the concentrating period, either a cross cue or a blank screen was shown, and

participants were instructed to either concentrate at the cross cue or rest while avoiding movements, respectively. For the cross cue, participants were instructed to imagine as if the cue was pulling them into the screen and they were consequently getting closer to the cue.

C. Experimental Task

The driving experiment was performed on a figure-8 track surrounded by walls, as shown in Fig. 5(b). Participants were seated on the mobility system and instructed to drive through the track. The driving route for the participants, which resembles the way the number is written, was the same for all experiments: starting from a corner of the track, they were expected to first drive the system forward toward the intersection, then proceed through the intersection of the other side and around the farther half to return to the intersection, then finally move back to the starting position by driving through the unvisited part of the track. The width of the track used in our experiment was uneven and varied throughout, making control of the mobility system and potential ways of traversal more complex.

Participants were initially given 15 minutes to complete each experiment. They were only instructed to complete the driving route as fast and safely as possible, and participants were able to freely observe their surroundings and determine whether they should rotate, move forward, or stop the mobility system on their own throughout all driving experiments. After this time, they were allowed to either continue or give up if they were stuck and too exhausted to complete the track.

D. Experimental Procedures

Considering that the velocity of our mobility system may slightly vary throughout the experiment due to our PID-based motor control, we asked participants to perform four different driving experiments to compare the performance of our proposed system. The experiments for each participant were held in a randomized order, with the first experiment held at least a day after the motor imagery and concentration training sessions. The four conditions were as follows.

1) *KBD-Only:* Participants controlled the system with a keyboard. The system rotated, stopped, or moved forward depending on the key pressed by the participants. Our shared control method using directional planning was not applied for this condition. The term KBD was used as an abbreviation to denote the use of a keyboard.
2) *KBD-DP:* Participants used a keyboard to drive the system. However, the shared control method proposed in this study was utilized in this condition. The term DP was used as an abbreviation to denote the use of directional planning.
3) *BCI-Only:* Participants were to drive the system using the BCI module. Only the positional PID-based directional path follower was used in this condition.
4) *BCI-DP:* Participants used the BCI module to drive the system with our directional planning-based shared control method. Except for using a different interface for control, this condition was the same as KBD-DP.

Unlike the BCI module, which required two consecutive commands to be the same in order to proceed with the corresponding movement, the commands were immediately reflected when driving with a keyboard. The mobility system was continuously and asynchronously controlled by the driver on the wheelchair for all four conditions, with collision avoidance being used considering the safety of participants.

E. Validation of BCI

Participants underwent a single motor imagery validation session before driving the system to train the classification model. The arrow cues were presented for a random duration, and participants were expected to perform corresponding motor imagery. The acquired data were used as a validation set to calibrate the classification model, and the model with the maximum validation accuracy was selected to drive the system. Participants with less than 75% maximum validation accuracy were discouraged from undergoing the experiment, as frequent misclassifications would result in erratic behavior of the system and could potentially cause dizziness or motion sickness.

To evaluate the concentration accuracy for each participant, we applied a sixfold cross-validation on our concentration classification model. We measured the true positive rate (TPR) and false discovery rate (FDR) as well as concentration classification accuracy to evaluate the discrimination of the concentrated state of participants. TPR and FDR were calculated as follows:

$$TPR = TP/(TP + FN) \qquad (9)$$

$$FDR = FP/(TP + FP) \qquad (10)$$

where TP, FN, and FP represent the numbers of true positives, false negatives, and false positives during cross-validation, respectively.

F. Evaluation of Driving Performance

To investigate the driving performance of participants during the four aforementioned conditions with our mobility system, we considered two different metrics for evaluation: how fast were the participants able to finish the given task, and how safe was the mobility system driven. Thus, the elapsed time, represented as the time taken for the participant to drive through the given task, and the path safety measures, calculated using the average distance from the mobility system to the nearest obstacle while driving, were used to compare the driving performance of participants during the given tasks.

V. RESULTS

As participants were only instructed to continuously and freely control the system to succeed on the given task, the actual intention of participants with respect to each command output could not be known and thus cannot directly measure the performance of BCI during the driving experiment. Alternatively, we investigated the performance of BCI on each individual by evaluating the data acquired prior to the driving experiment. To also provide insight on how each participant navigated the system under the four given conditions, the trajectories participants underwent were conveyed.

TABLE I
MOTOR IMAGERY AND CONCENTRATION EVALUATION RESULTS

Participant	MI Sessions	MI Validation Acc (%)	Concentration		Concentration Acc (%)
			TPR (%)	FDR (%)	
S1	8	79.30	85.85	42.95	60.08
S2	8	79.22	86.26	35.17	69.43
S3	6	85.87	87.97	36.13	68.46
S4	6	81.69	79.92	27.23	74.51
S5	7	91.15	88.05	39.13	65.44
AVG	-	**83.45**	**85.61**	**36.12**	**67.58**

TABLE II
TIME TO COMPLETION FOR EACH EXPERIMENT

Participant	KBD-Only (s)	KBD-DP (s)	BCI-Only (s)	BCI-DP (s)
S1	346	299	null (>15min)	518
S2	355	316	null (>15min)	555
S3	356	308	898	495
S4	374	311	1033 (>15min)	684
S5	382	312	null (>15min)	549
AVG	**362.6**	**309.2**	**-**	**560.2**
STD	**13.29**	**5.71**	**-**	**65.59**
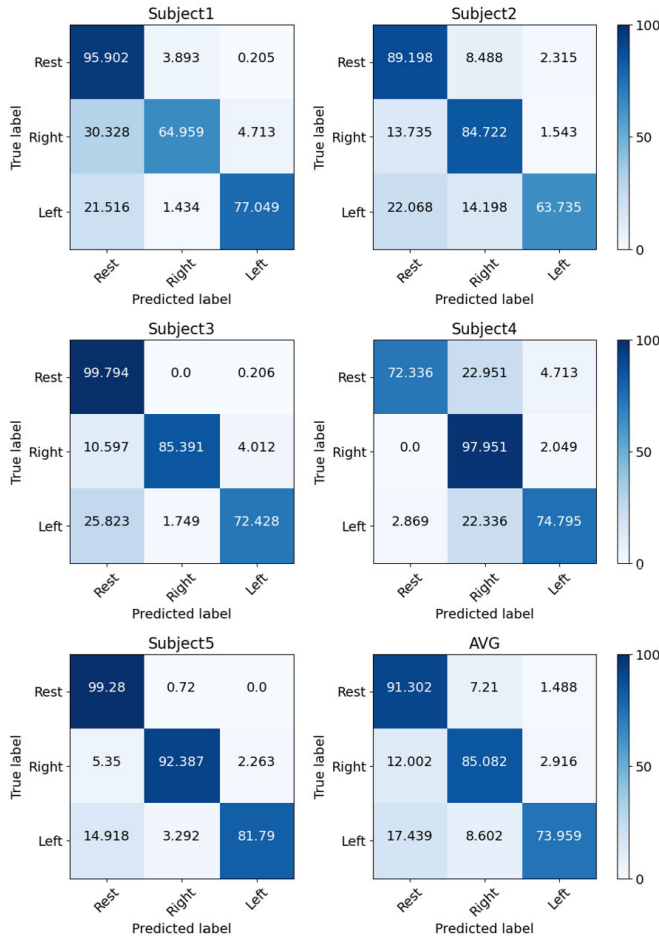
Fig. 6. Validation accuracies of the used models from participants regarding three motor imagery states.

A. Validation Results of BCI Classification

The number of training sessions each participant underwent and their maximum validation accuracy for motor imagery while training with the data from the training and validation sessions are shown in Table I. The average maximum validation accuracy for the participants was 83.45%, with participant S2 achieving the lowest validation accuracy of 79.22%, which was higher than our determined threshold of 75% for controlling the mobility system.

Fig. 6 further presents the confusion matrices that include validation accuracies from the used models of classifying

left-hand grasping, right-hand grasping, and resting state motor imagery for each participant. The results showed that for four out of five participants, our BCI module was able to discriminate the resting task most accurately out of the three possible motor imagery classes. Participant S4 in contrast showed the lowest accuracy while performing resting state motor imagery with an accuracy rate of 72.34%.

Table I also shows the cross-validated TPR and FDR results as well as the classification accuracy rate of each participant for concentration. The average TPR and FDR rates for the participants were 85.61% and 36.12%, respectively, and the average concentration accuracy was 67.58%.

B. Performance Results for Keyboard Experiments

The times taken to finish the two keyboard experiments are shown in Table II. The average time taken for the KBD-Only experiment was 362.6 s, which was longer than the average time taken for the KBD-DP experiment of 309.2 s. The standard deviation was also greater for KBD-Only at 13.29 compared to KBD-DP's 5.71, showing greater variability for participants in KBD-Only. All five participants finished both experiments within the 15-min limit but showed faster completion for the KBD-DP experiment than for the KBD-Only experiment.

C. Performance Results for BCI Experiments

The times for the two BCI experiments are also shown in Table II. As can be seen from the results, only two participants out of the five were able to complete BCI-Only, with one participant finishing after 15 min. The sole participant who was able to complete the task within the given time took 898 s.

By contrast, all participants were able to finish BCI-DP within the given time, which represent the results for when using BCI along with our shared control approach. The average time taken for BCI-DP was 560.2 s with a standard deviation of 65.59, inevitably showing more variability within participants compared to both keyboard experiments. With participant S4 taking the longest time of 684 s and all participants finishing the track faster than BCI-Only, the results of using our shared control method narrowed the gap between using the keyboard interface and using asynchronous BCI without the shared control support.
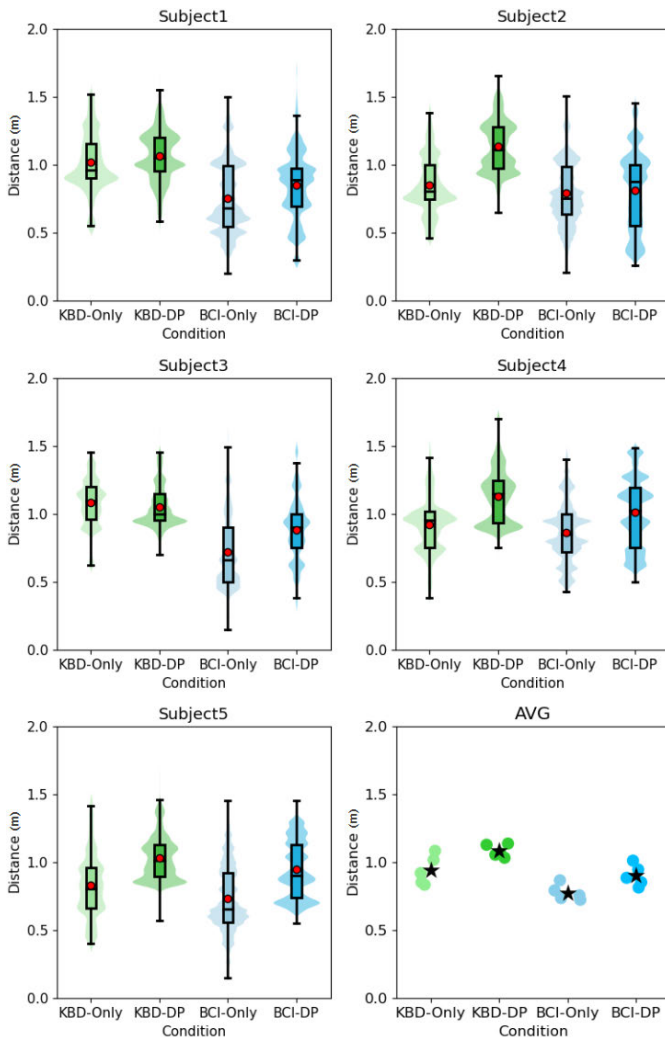
Fig. 7. Measured distance between the mobility system and the nearest obstacles throughout each driving task.

D. Path Safety Measures

The path safety measures indicating the average distance between the mobility system and the nearest obstacle throughout each driving task are shown in Fig. 7. As can be seen in Fig. 7, participants maintained the greatest grand average distance of approximately 1.08 m during KBD-DP. The grand average distances for KBD-Only and BCI-DP came close at 0.94 and 0.90 m, respectively. The grand average distances for KBD-Only and BCI-DP were within each other's standard deviations, with two participants S4 and S5 recording larger distances during BCI-DP. Finally, BCI-Only had the shortest distance of approximately 0.77 m.

VI. DISCUSSION

The aim of this study was to provide drivers with intuitive and direct control over the mobility system while preserving their authority throughout the entire driving period. We built a mobility system that continuously maps motor imagery and concentration to different driving commands, enabling drivers to perform intuitive and direct asynchronous control with only their brain signals. As such motor imagery-based BCIs are prone to frequent errors, we proposed a shared control method suitable for asynchronous BCIs to make the mobility system

more resistant to misclassifications. Furthermore, our system could be applied to unfamiliar places and environments that the mobility system never visited before, as we did not provide any environmental information toward the goal point prior to conducting our driving tasks.

The results of our driving experiment showed that our shared control approach and directional planning algorithm led to an improved driving performance by exhibiting higher task completion and increasing safety. All participants successfully completed BCI-DP within the given time, while only two participants finished BCI-Only with one finishing within 15 minutes limit. With participants maintaining a larger distance from obstacles in BCI-DP than BCI-Only, our shared control approach also exhibits greater safety by lowering the chance of collision. It is also noteworthy that the average distances for BCI-DP were quite similar to those for KBD-Only, with two participants managing to take paths further from the obstacles in BCI-DP.

Although the performances for BCI-DP did not exceed the performances for the keyboard experiments, our study still shows the potential of using BCI with shared control for real-world mobility systems. Along with the trajectories shown in Fig. 8 for each driving condition, it can be observed in our results that using the shared control approach for both types of interfaces resulted in a reduction of both the variability of driving performance in elapsed time and the complexity of the system's movement throughout navigation, which suggests that our method reduces the system's reliance on BCI's classification accuracy. In terms of the difference in trajectories between BCI and the keyboard, it becomes more clear that the navigation performance between the two interfaces was narrowed upon the application of shared control for our experiment. The reduction of unstabilized movement, particularly noticeable in BCI compared to the keyboard, indicates a decrease in the user's efforts to precisely direct the wheelchair. The trajectory results thus demonstrate that precise control is less demanding when our shared control is in effect, which is a necessary component for interfaces like BCIs that are error-prone.

Our shared control approach effectively enhanced navigation performance for asynchronous BCI in terms of elapsed time for task completion, with all participants taking only approximately twice as long for BCI-DP as they did for the two keyboard experiments, and most failing to complete BCI-Only. This result also signifies the narrowing of the gap between driving with brain signals and using other widely used interfaces, as our study's elapsed time gap is substantially smaller compared to previous studies that also compared BCI with other interfaces such as keyboards or joysticks [11], [12], [27]. Unlike previous studies that typically consumed more than twice the average task completion time for BCIs compared to other commonly used interfaces, and in some cases relied on external stimuli or utilized additional biosignals alongside brain signals, our approach offers practicality by eliminating the need for external stimuli and achieved improvements with asynchronous BCI that produces commands solely from the user's thoughts. Our mobility system therefore lessens the gap between the two interfaces for driving

One of the unexpected issues from our study that negatively affected control performance for our BCI system was the discrimination of the user's concentration state, which was used to intuitively map with forward movement. Participants may have found differentiating between concentrating and not concentrating difficult as there is no clear definition of what the thought of moving forward entails, unlike other concentration tasks such as reading or solving questions [28], [29]. New intuitive paradigms that help participants with eliciting signals corresponding to concentration tasks may need to be developed to improve intuitive driving, similar to various training and control protocols with motor imagery [4], [30], [31]. State-of-the-art BCIs are also affected by changes in mental states and other psychological factors [32], [33]. Negative emotions such as anxiety, frustration, or distress elicited by various driving situations, including but not limited to the system suddenly stopping due to a detected obstacle, the mobility system misbehaving due to misclassifications, and the mobility system rotating too frequently, may have caused deterioration in motor imagery performance [34], [35], [36]. Unlike simulated scenarios in which the driver's safety is guaranteed or experiments similar to BCI-DP in which control policies try to maximize the distance to obstacles, the BCI-Only experiment is more prone to these situations, which could have negatively affected the participants by causing frequent emotional changes.

As this study is merely a step toward a system that gives the driver direct, intuitive control by mapping the imagination of hand movements to rotations of our mobility system while supporting BCI's error-prone problem with shared control capabilities, further work must be done to reach the final goal of providing a control experience so intuitive that users feel as if the mobility system was a natural extension of their body. Our system currently gives a limited number of commands and control options to the driver, as the degree of directional movement and velocity cannot be adjusted by the users themselves. Research on giving the driver more control, perhaps by using the strength of neural patterns to change the velocity and directional degree with which the system moves, would prove to be beneficial for achieving such a system. Developing better classification models for BCIs would also solve the issues caused by low BCI accuracy. Finally, although the system introduced in this study aimed to provide intuitive control and preserve the authority of control for drivers, drivers may possibly experience fatigue as the system requires them to maintain motor imagery or remain focused to sustain its corresponding operation. Thus, further work on improving the semiautonomous driving experience for asynchronous BCI-based control should be explored to lessen the workload of drivers while maintaining their dominance over the system.

There are also some existing limitations in our experiment. A small sample size due to our criteria of permitting only participants with discriminant brain patterns is one instance. Our future research will thus conduct an investigation into different experimental designs aimed at training users to produce improved brain signals related to motor imagery and forward movement of the device, which will involve diverse groups of participants including those with disabilities.

Fig. 8. Driving trajectories of the participants during the four different experimental tasks. The initial position of the mobility system is marked with a red dot, and participants were to reach the green area to finish the experimental task.

in terms of both safety and performance, taking a step toward the application of BCI-based mobility systems in real life, which would be helpful especially for people with motor disabilities.

Time restrictions for the driving experiment may serve as another limitation, as participants had to drive the mobility system in all four conditions and extensive experiment time would cause fatigue while driving the system. Such limitations and constraints for our experimental design were inevitable for our study as the safety of participants was considered as our top priority.

VII. CONCLUSION

In this study, we proposed an asynchronous BCI-based mobility system that utilizes motor imagery and concentration to directly map the driver's intentions for control while addressing its error-prone challenges with shared control capabilities using LiDAR and IMU sensors. The experimental results indicate that the shared control approach not only facilitates users who would otherwise struggle to operate the system with BCIs to accomplish the driving task successfully but also enhances both safety and elapsed time for navigation in real-life environments. Our approach narrows the gap between driving using neural signals and driving using a keyboard, offering valuable insights for future asynchronous BCI-based mobility systems. This represents a step forward in allowing users to drive with their thoughts while retaining control authority throughout the entire operation.

ACKNOWLEDGMENT

REFERENCES

[1] M. A. Khan, R. Das, H. K. Iversen, and S. Puthusserypady, "Review on motor imagery based BCI systems for upper limb post-stroke neurorehabilitation: From designing to application," *Comput. Biol. Med.*, vol. 123, Aug. 2020, Art. no. 103843.

[2] C. Zuo et al., "Novel hybrid brain–computer interface system based on motor imagery and P300," *Cogn. Neurodyn.*, vol. 14, no. 2, pp. 253–265, Apr. 2020.

[3] S. Nagel and M. Spüler, "Asynchronous non-invasive high-speed BCI speller with robust non-control state detection," *Sci. Rep.*, vol. 9, no. 1, pp. 1–9, Jun. 2019.

[4] J. W. Choi, S. Huh, and S. Jo, "Improving performance in motor imagery BCI-based control applications via virtually embodied feedback," *Comput. Biol. Med.*, vol. 127, Dec. 2020, Art. no. 104079.

[5] J.-H. Jeong, K.-H. Shim, D.-J. Kim, and S.-W. Lee, "Brain-controlled robotic arm system based on multi-directional CNN-biLSTM network using EEG signals," *IEEE Trans. Neural Syst. Rehabil. Eng.*, vol. 28, no. 5, pp. 1226–1238, May 2020.

[6] Y. Chae, J. Jeong, and S. Jo, "Toward brain-actuated humanoid robots: Asynchronous direct control using an EEG-based BCI," *IEEE Trans. Robot.*, vol. 28, no. 5, pp. 1131–1144, Oct. 2012.

[7] H. Gao et al., "EEG-based volitional control of prosthetic legs for walking in different terrains," *IEEE Trans. Autom. Sci. Eng.*, vol. 18, no. 2, pp. 530–540, Apr. 2021.

[8] X. Fan, L. Bi, T. Teng, H. Ding, and Y. Liu, "A brain–computer interface-based vehicle destination selection system using P300 and SSVEP signals," *IEEE Trans. Intell. Transp. Syst.*, vol. 16, no. 1, pp. 274–283, Feb. 2015.

[9] R. Zhang et al., "Control of a wheelchair in an indoor environment based on a brain–computer interface and automated navigation," *IEEE Trans. Neural Syst. Rehabil. Eng.*, vol. 24, no. 1, pp. 128–139, Jan. 2016.

[10] Y. Yu, Y. Liu, J. Jiang, E. Yin, Z. Zhou, and D. Hu, "An asynchronous control paradigm based on sequential motor imagery and its application in wheelchair navigation," *IEEE Trans. Neural Syst. Rehabil. Eng.*, vol. 26, no. 12, pp. 2367–2375, Dec. 2018.

[11] V. Sakkalis, M. Krana, C. Farmaki, C. Bourazanis, D. Gaitatzis, and M. Pediaditis, "Augmented reality driven steady-state visual evoked potentials for wheelchair navigation," *IEEE Trans. Neural Syst. Rehabil. Eng.*, vol. 30, pp. 2960–2969, 2022.

[12] K.-T. Kim, H.-I. Suk, and S.-W. Lee, "Commanding a brain-controlled wheelchair using steady-state somatosensory evoked potentials," *IEEE Trans. Neural Syst. Rehabil. Eng.*, vol. 26, no. 3, pp. 654–665, Mar. 2018.

[13] M. Liu et al., "Indoor simulated training environment for brain-controlled wheelchair based on steady-state visual evoked potentials," *Frontiers Neurorobot.*, vol. 13, p. 101, Jan. 2020.

[14] Y. Yu et al., "Self-paced operation of a wheelchair based on a hybrid brain-computer interface combining motor imagery and P300 potential," *IEEE Trans. Neural Syst. Rehabil. Eng.*, vol. 25, no. 12, pp. 2516–2526, Dec. 2017.

[15] A. Cruz, G. Pires, A. Lopes, C. Carona, and U. J. Nunes, "A self-paced BCI with a collaborative controller for highly reliable wheelchair driving: Experimental tests with physically disabled individuals," *IEEE Trans. Human-Mach. Syst.*, vol. 51, no. 2, pp. 109–119, Apr. 2021.

[16] A. A. Nooh, J. Yunus, and S. M. Daud, "A review of asynchronous electroencephalogram-based brain computer interface systems," in *Proc. Int. Conf. Biomed. Eng. Technol. (IPCBEE)*, vol. 11, 2011, pp. 55–59.

[17] M. Ahn, M. Lee, J. Choi, and S. Jun, "A review of brain-computer interface games and an opinion survey from researchers, developers and users," *Sensors*, vol. 14, no. 8, pp. 14601–14633, Aug. 2014.

[18] K. Nakayashiki, M. Saeki, Y. Takata, Y. Hayashi, and T. Kondo, "Modulation of event-related desynchronization during kinematic and kinetic hand movements," *J. Neuroeng. Rehabil.*, vol. 11, no. 1, p. 90, Dec. 2014.

[19] G. Pfurtscheller, C. Brunner, A. Schlögl, and F. H. L. D. Silva, "Mu rhythm (de)synchronization and EEG single-trial classification of different motor imagery tasks," *NeuroImage*, vol. 31, no. 1, pp. 153–159, May 2006.

[20] S. Lim, M. Yeo, and G. Yoon, "Comparison between concentration and immersion based on EEG analysis," *Sensors*, vol. 19, no. 7, p. 1669, Apr. 2019.

[21] R. T. Schirrmeister et al., "Deep learning with convolutional neural networks for EEG decoding and visualization," *Hum. Brain Mapping*, vol. 38, no. 11, pp. 5391–5420, Nov. 2017.

[22] J. A. K. Suykens and J. Vandewalle, "Least squares support vector machine classifiers," *Neural Process. Lett.*, vol. 9, no. 3, pp. 293–300, Jun. 1999.

[23] K. Yaomanee, S. Pan-Ngum, and P. I. N. Ayuthaya, "Brain signal detection methodology for attention training using minimal EEG channels," in *Proc. 10th Int. Conf. ICT Knowl. Eng.*, Nov. 2012, pp. 84–89.

[24] W. Hess, D. Kohler, H. Rapp, and D. Andor, "Real-time loop closure in 2D LiDAR SLAM," in *Proc. IEEE Int. Conf. Robot. Autom. (ICRA)*, May 2016, pp. 1271–1278.

[25] G. Beraldo, L. Tonin, J. D. R. Millán, and E. Menegatti, "Shared intelligence for robot teleoperation via BMI," *IEEE Trans. Human-Mach. Syst.*, vol. 52, no. 3, pp. 400–409, Jun. 2022.

[26] K. H. Ang, G. Chong, and Y. Li, "PID control system analysis, design, and technology," *IEEE Trans. Control Syst. Technol.*, vol. 13, no. 4, pp. 559–576, Jul. 2005.

[27] N. Siribunyaphat and Y. Punsawad, "Brain–computer interface based on steady-state visual evoked potential using quick-response code pattern for wheelchair control," *Sensors*, vol. 23, no. 4, p. 2069, Feb. 2023.

[28] N.-H. Liu, C.-Y. Chiang, and H.-C. Chu, "Recognizing the degree of human attention using EEG signals from mobile sensors," *Sensors*, vol. 13, no. 8, pp. 10273–10286, Aug. 2013.

[29] L.-W. Ko, O. Komarov, W.-K. Lai, W.-G. Liang, and T.-P. Jung, "Eyeblink recognition improves fatigue prediction from single-channel forehead EEG in a realistic sustained attention task," *J. Neural Eng.*, vol. 17, no. 3, Jun. 2020, Art. no. 036015.

[30] J. W. Choi, B. H. Kim, S. Huh, and S. Jo, "Observing actions through immersive virtual reality enhances motor imagery training," *IEEE Trans. Neural Syst. Rehabil. Eng.*, vol. 28, no. 7, pp. 1614–1622, Jul. 2020.

[31] M. Song and J. Kim, "A paradigm to enhance motor imagery using rubber hand illusion induced by visuo-tactile stimulus," *IEEE Trans. Neural Syst. Rehabil. Eng.*, vol. 27, no. 3, pp. 477–486, Mar. 2019.

[32] B. H. Kim, S. Koh, S. Huh, S. Jo, and S. Choi, "Improved explanatory efficacy on human affect and workload through interactive process in artificial intelligence," *IEEE Access*, vol. 8, pp. 189013–189024, 2020.

[33] A. Appriou, A. Cichocki, and F. Lotte, "Modern machine-learning algorithms: For classifying cognitive and affective states from electroencephalography signals," *IEEE Syst., Man, Cybern. Mag.*, vol. 6, no. 3, pp. 29–38, Jul. 2020.

[34] A. Chaudhuri and A. Routray, "Driver fatigue detection through chaotic entropy analysis of cortical sources obtained from scalp EEG signals," *IEEE Trans. Intell. Transp. Syst.*, vol. 21, no. 1, pp. 185–198, Jan. 2020.

[35] U. Talukdar, S. M. Hazarika, and J. Q. Gan, "Motor imagery and mental fatigue: Inter-relationship and EEG based estimation," *J. Comput. Neurosci.*, vol. 46, no. 1, pp. 55–76, Feb. 2019.

[36] H. S. Kim, D. Yoon, H. S. Shin, and C. H. Park, "Predicting the EEG level of a driver based on driving information," *IEEE Trans. Intell. Transp. Syst.*, vol. 20, no. 4, pp. 1215–1225, Apr. 2019.

Jin Woo Choi received the B.S., M.S., and Ph.D. degrees in computer science from the Korea Advanced Institute of Science and Technology (KAIST), Daejeon, Republic of Korea, in 2017, 2019, and 2022, respectively.

He is currently a Postdoctoral Researcher with the Department of Neurology and Neurological Sciences, Stanford University School of Medicine, Stanford, CA, USA. His research interests include brain–computer interfaces, machine learning, intelligent systems, deep-learning applications, and virtual reality.

Junyong Park received the B.S. and M.S. degrees in computer science from the Korea Advanced Institute of Science and Technology (KAIST), Daejeon, Republic of Korea, in 2018 and 2020, respectively, where he is currently pursuing the Ph.D. degree with the School of Computing.

His research interests include human–robot interactions, computer vision, robotics, machine learning, and intelligent systems.

Sejoon Huh received the B.S. and M.S. degrees in computer science from the Korea Advanced Institute of Science and Technology (KAIST), Daejeon, Republic of Korea, in 2019 and 2021, respectively, where he is currently pursuing the Ph.D. degree with the School of Computing.

His research interests are brain–computer interface applications and applied machine learning.

Sungho Jo received the B.S. degree from the School of Mechanical and Aerospace Engineering, Seoul National University, Seoul, Republic of Korea, in 1999, and the S.M. degree in mechanical engineering and the Ph.D. degree in electrical engineering and computer science from the Massachusetts Institute of Technology (MIT), Cambridge, MA, USA, in 2001 and 2006, respectively.

While pursuing the Ph.D., he was associated with the Computer Science and Artificial Intelligence Laboratory (CSAIL), Laboratory for Information Decision and Systems (LIDS), and Harvard–MIT HST NeuroEngineering Collaborative. Before joining the faculty of the Korea Advanced Institute of Science and Technology (KAIST), Daejeon, Republic of Korea, he was a Postdoctoral Researcher with the MIT Media Laboratory. Since December 2007, he has been with the School of Computing, KAIST, where he is currently a Professor. His research interests include intelligent robots, neural interfacing computing, and wearable computing.